Available online at www.sciencedirect.com
SCIENCE DIRECT®
Journal of Catalysis 223 (2004) 340–351
JOURNAL OF CATALYSIS
www.elsevier.com/locate/jcat

Steam reforming of methanol to H_2 over nonreduced Zr-containing CuO/ZnO catalysts

Paul H. Matter, Drew J. Braden, and Umit S. Ozkan *

The Ohio State University, Department of Chemical Engineering, 140 W 19th Avenue, Columbus, OH 43210, USA

Received 20 October 2003; revised 22 January 2004; accepted 28 January 2004

Abstract

Zr-containing CuO/ZnO catalysts are examined for their use in the reaction of methanol with water to produce hydrogen. Catalyst samples with varying compositions were prepared by means of a coprecipitation method, and the effect of different pretreatment conditions was examined. Activity testing shows that the catalysts do not require prereduction to obtain good activity for the steam reforming of methanol, although prereduction with diluted H_2 increases activity in some cases. The catalysts were characterized using BET surface area analysis, Cu surface area analysis, temperature-programmed reduction (TPR), temperature-programmed desorption (TPD), thermo-gravimetric analysis with differential scanning calorimetry (TGA/DSC), X-ray diffraction (XRD), and X-ray photoelectron spectroscopy (XPS). Characterization suggests that the most active steam-reforming catalysts initially consist of CuO, ZnO, and a high surface area amorphous phase of zirconia that contains carbonates; however, partial reduction of surface copper during the reaction is apparent from XPS results.
© 2004 Elsevier Inc. All rights reserved.

Keywords: Methanol steam reforming; Hydrogen production; Copper catalysts; Zirconia

1. Introduction

Methanol is potentially a good source of hydrogen for mobile fuel cells since it is a liquid at ambient conditions, has a high hydrogen to carbon ratio, and can be converted to hydrogen using either steam or oxygen at relatively low temperatures compared to other fuels. The steam reforming of methanol (SRM) and the partial oxidation of methanol (POM) reactions are shown here with heat of reactions at STP:

$$\text{SRM,}\quad CH_3OH_{(l)} + H_2O_{(l)} \rightarrow CO_2 + 3H_2 \quad (\Delta H_{rxn} = 130.9\ \text{kJ/mol});$$

$$\text{POM,}\quad CH_3OH_{(l)} + \tfrac{1}{2}O_2 \rightarrow CO_2 + 2H_2 \quad (\Delta H_{rxn} = -154.9\ \text{kJ/mol}).$$

The SRM reaction produces 3 mol of hydrogen per mole of fuel, while the POM produces only 2. However, the efficiency of the SRM reaction is hindered by its endothermicity since heat must be provided for the reaction to run. Combining the two reactions for the oxidative steam reforming of methanol (OSRM) reaction is potentially the best option for mobile hydrogen production. The maximum theoretical efficiency based on the lower heating value (LHV) of H_2 produced compared to the fuel consumed is obtained for the autothermal reaction in which enough oxygen is used to make the heat of reaction zero. Theoretically, methanol can be converted to hydrogen with better efficiency than any other hydrocarbon being considered for on-board hydrogen production [1]. The use of methanol to produce hydrogen is also attractive because of the relatively low selectivity to by-products such as carbon monoxide and methane compared to alkane or higher alcohol reforming.

$Cu/ZnO/Al_2O_3$ catalysts have been extensively studied for the methanol synthesis reaction, the water gas-shift reaction, steam reforming of methanol, and the partial oxidation of methanol [2–17]. Cu is believed to be the active phase in these catalysts, since activity is typically proportional to Cu surface area. ZnO is known to improve the dispersion of copper and also its reducibility, which may be important if a redox reaction mechanism occurs [18]. Additionally, the importance of ZnO may be explained by spillover effects [19,20]. The ability of ZnO to store hydrogen and transport species to the Cu phase has been demonstrated to have favorable consequences for many of the aforementioned re-

* Corresponding author.
E-mail address: ozkan.1@osu.edu (U.S. Ozkan).

0021-9517/$ – see front matter © 2004 Elsevier Inc. All rights reserved.
doi:10.1016/j.jcat.2004.01.031

actions. The addition of Al_2O_3 improves the surface area and slows the sintering of the catalyst. Moreover, Al_2O_3 could contribute to advantageous spillover effects, although ZnO apparently has more advantageous effects with the Cu phase. Shortcomings of these catalysts have been noted as the need for a prereaction reduction to induce activity, low resistance to contaminants, and problems with long-term stability [6].

Copper supported by zirconia rather than zinc oxide or alumina has also shown good activity for the methanol synthesis reaction, the reverse of methanol reforming [21,22]. Similarly to ZnO, ZrO_2 improves the reducibility of CuO. Compared to alumina, zirconia has the advantage of possessing activity by itself or when used as a support for copper. Additionally, ZrO_2 is capable of adsorbing methanol, making it an attractive support material for reforming catalysts [23].

More recently, zirconia-containing copper-based catalysts have shown promising activity for the SRM and the OSRM reactions [14,24–28]. Breen and Ross studied the steam reforming of methanol using prereduced zirconia-containing $Cu/ZnO/Al_2O_3$ catalysts [24]. They found that using zirconia as a support for Cu and ZnO produces a more active catalyst than $Cu/ZnO/Al_2O_3$ for the SRM reaction. The stability of the catalyst was improved if a small amount of Al_2O_3 was added, most likely because the amorphous zirconia phase was stabilized. Velu et al. studied the OSRM reaction over prereduced zirconia-containing $Cu/ZnO/Al_2O_3$ catalysts [25]. This group established that ZrO_2 is also a better support for OSRM. The better performance of zirconia-containing catalysts was attributed to a higher Cu surface area, better Cu dispersion, and improved reducibility of Cu compared to $Cu/ZnO/Al_2O_3$ catalysts.

The prereduction of $Cu/ZnO/Al_2O_3$ catalysts is necessary to obtain maximum activity. This reduction must be carried out carefully in a diluted hydrogen stream with a slow heating rate in order to prevent catalyst sintering during the highly exothermic reduction of CuO to Cu^0. However, the previously studied reactions for these catalysts (i.e., the water–gas-shift and methanol synthesis reactions) are typically carried out in stationary large-scale operations where prereduction is not as much of a burden. In this study we examine the activity of these catalysts without prereduction, since this type of treatment would be inconvenient for mobile fuel cell systems. Only the SRM, the reforming reaction with the slowest kinetics, is examined in this study. Characterization of the prereaction catalysts using TPR, N_2O passivation, XRD, TPD, TGA/DSC, and XPS techniques is presented, as well as postreaction XPS.

2. Experimental methods

2.1. Catalyst preparation

The catalysts were prepared using a coprecipitation technique similar to the one described by Breen and Ross [24]. First, 1.25 M solutions of Cu, Zn, and ZrO nitrates were mixed and then precipitated using 0.25 M Na_2CO_3 added dropwise under vigorous stirring at room temperature, while the pH was maintained at 8.5. For some samples an alternative base was used to carry out the precipitation. After an additional 30 min of stirring the precipitate was then washed using suction filtration and 2 L of hot double-distilled water to remove Na^+ and any remaining soluble salts. The precursor was then dried overnight at 100 °C, crushed to a fine powder, and calcined. Calcination was carried out in a tube furnace using air or N_2 flowing at 50 sccm. The temperature was ramped from 25 °C to the maximum temperature at a rate of 5 °C/min. The maximum calcination temperature varied between 350 and 550 °C for different samples and was held constant for 4 h. If the catalyst was prereduced, it was done in situ at 250 °C using 5% H_2 in N_2 flowing at 20 sccm for 3 h before activity testing. Surface area was determined by N_2 physisorption using a Micromeritics ASAP 2010 adsorption instrument.

2.2. TPR/Cu surface area measurements

The specific Cu surface area was measured for some selected catalysts by a N_2O passivation method, using an in-house constructed system described elsewhere [29]. First, samples were calcined in situ for 1 h with 20% O_2 in He (50 sccm total flow) at the same calcination temperature used during catalyst preparation. Next, the catalysts were reduced with 5% H_2 in N_2 while ramping the temperature from 25 to 350 °C at 5 °C/min. H_2 consumption was monitored with a TCD, and was subsequently used to estimate the copper content of the catalyst by comparison to a pure CuO reference. The temperature was then lowered to 60 °C and pulses of N_2O diluted ($< 20\%$) in He were passed over the sample. The decomposition of N_2O to N_2 was monitored with the online HP 5890 II GC-MS. The sample then underwent a second reduction up to 350 °C. The Cu surface area was calculated assuming that CuO was reduced to Cu^0 during the first reduction. Additionally, it is assumed that in the proceeding step surface Cu is oxidized to Cu_2O at a much faster rate than it is oxidized to CuO or than the subsurface is oxidized. This method must also assume 1.46×10^{19} Cu atoms/m^2 to calculate Cu surface area from the amount of N_2O adsorbed. All of these assumptions are commonly used by researchers for measuring the Cu surface area of supported samples [30–32].

2.3. XRD

Powder X-ray diffraction patterns were obtained using a Bruker D8 X-ray diffractometer equipped with an HTK 1200 sample holder capable of controlling temperature and atmosphere. The X-ray source was Cu-K_α radiation. Diffraction patterns were obtained for all samples after calcination. For selected samples, patterns were obtained during in situ calcination and reduction steps. In these experiments

the temperature was ramped between measurements at a rate of 5 °C/min with a 5-min pause at each temperature before recording the pattern. Patterns for the precursor to catalyst transition were recorded every 50 °C while open to the atmosphere. For reduction, the catalyst was exposed to 5% H_2 in N_2 flowing at 10 sccm and diffraction patterns were recorded every 25 °C beginning at 100 up to 350 °C.

2.4. TPD

Temperature-programmed desorption studies were conducted using the previously described in-house built system with online GC-MS. The sample (100 mg, powder) was placed in a glass U-tube, sandwiched between plugs of silica wool for support. The sample was then cleaned by heating to the calcination temperature of the sample in He flowing at 30 sccm. For blank TPD experiments the temperature was increased from room temperature to 850 °C at a rate of 10 °C/min while using He as a carrier (flow = 20 sccm). Desorbing species were detected by the GC-MS.

2.5. TGA/DSC

Thermo-gravimetric analysis with differential scanning calorimetry experiments were conducted using a Setaram TG-DSC111 with the effluent gas connected to an online HP 5890II GC-MS. For the precursor decomposition experiments approximately 20 mg of washed and dried precursor was placed in a quartz crucible and loaded into the TGA/DSC. The temperature was then raised from 25 to 800 °C at a rate of 5 °C/min under an approximate He flow of 40 sccm. Changes in weight and heat flow were detected with the TGA/DSC, while the major effluents produced (CO_2, H_2O, and O_2) were detected by the GC-MS.

2.6. Activity testing

Activity testing was conducted in an in-house-constructed reactor system with an online HP5890 GC equipped with a TCD and FID for determining product composition. The FID was equipped with a methanizer to allow detection of CO down to 10 ppm. For equal weight testing, 50 mg of the powder catalyst sample was loaded in a 5 mm i.d., 316 SS tube, while for equal surface area tests 4.4 m^2 of catalyst was used. The reactor tube was then encased in an in-house-built furnace. A thermocouple measured the temperature at the bottom of the silica wool that supported the catalyst in the downward flow scheme. For all steam-reforming tests the total flow rate was 100 sccm, with a composition of 15.5% methanol, 19.4% water, 36.9% N_2, and the balance Ar carrier. Both N_2 and Ar were bubbled through their respective controlled temperature-saturation chamber containing water or methanol in order to achieve the desired feed composition. Steady-state measurements were taken at least 4 h after beginning flow to the reactor, at which point the product composition was stable. Data were taken at 200, 220, 250, and 300 °C. Lower temperatures were recorded first, and at least 4 h were given to reach steady state between temperature adjustments. For time on stream tests, 50 mg of catalyst was used and the temperature was held steady at 250 °C. If the catalyst was prereduced it was done in situ at 250 °C using 5% H_2 in N_2 flowing at 20 sccm immediately before beginning the reaction. Comparisons between catalysts are made with H_2 yield, defined as the percentage of theoretical H_2 produced based on all the methanol fed being converted to H_2 by the SRM.

2.7. XPS

X-ray photoelectron spectra were recorded using an AXIS Ultra XPS with a Mg anode operating at 14 kV and 10 mA. The powder sample was supported by either double-sided carbon tape or stainless-steel disks. Charge-shift corrections were made by assuming a C 1s signal of 284.5 eV. Postreduction and postreaction samples were sealed in He before the sample temperature was lowered to room temperature. A glove box and controlled atmosphere transfer chamber were used to ensure that the samples were not exposed to atmospheric conditions before analysis.

3. Results and discussion

3.1. Physical properties

A list of the catalysts prepared and the respective preparation parameters and physical properties for each catalyst are reported in Table 1. Parameters that were varied during catalyst preparation included Cu content, Zn:Zr ratio, calcination temperature, base used for precipitation, and addition of aluminum. The addition of zirconia to Cu/Zn had an advantageous effect on surface area, and the addition of a small amount of Al_2O_3 improved surface area even more. These higher surface areas can be attributed to the presence of an amorphous zirconium phase. Aluminum could improve the surface area by stabilizing the amorphous zirconium and by preventing CuO and ZnO sintering during the calcination. Surface area was lost with increasing calcination temperature, while using an alternative base did not affect surface area as long as carbonates were present.

3.2. TPR/Cu surface area

The addition of ZnO or ZrO_2 lowered the reduction temperature of CuO pronouncedly compared to its pure form, as shown in Fig. 1. The reduction peak for CZZ-433 (350) is much sharper and ends at a lower temperature than the other samples possibly because of the better Cu dispersion in this sample. A more detailed analysis of similar materials has been performed by other researchers [18,24]. Only the CuO phase is reduced to its metallic form under the conditions of the TPR used here. The results of the Cu surface

Table 1
Catalyst naming scheme and preparation conditions

Catalyst name	Precursor (mol%)				Base used in	Calcination	BET surface
	Cu	Zn	Zr	Al	preparation	temperature (°C)	area (m^2/g)
Cu/Zn (350)	50.0	50.0	–	–	Na_2CO_3	350	22
Cu/Zr (350)	50.0	–	50.0	–	Na_2CO_3	350	86
Cu/Zr (550)	50.0	–	50.0	–	Na_2CO_3	550	43
CZZ-244 (350)	20.0	40.0	40.0	–	Na_2CO_3	350	75
CZZ-244 (450)	20.0	40.0	40.0	–	Na_2CO_3	450	66
CZZ-244 (550)	20.0	40.0	40.0	–	Na_2CO_3	550	52
CZZ-424 (350)	40.0	20.0	40.0	–	Na_2CO_3	350	49
CZZ-442 (350)	40.0	40.0	20.0	–	Na_2CO_3	350	58
CZZ-433 (350)	40.0	30.0	30.0	–	Na_2CO_3	350	89
CZZ-433 KC (350)	40.0	30.0	30.0	–	K_2CO_3	350	91
CZZ-433 AmC (350)	40.0	30.0	30.0	–	$(NH_4)_2CO_3$	350	88
CZZ-433 AmOH (350)	40.0	30.0	30.0	–	NH_4OH	350	68
CZZ-433 (450)	40.0	30.0	30.0	–	Na_2CO_3	350	66
CZZ-433 (550)	40.0	30.0	30.0	–	Na_2CO_3	550	39
CZZA-433:0.5 (350)	38.1	28.6	28.6	4.8	Na_2CO_3	350	123
CZZA-433:1.5 (350)	34.8	26.1	26.1	13.0	Na_2CO_3	350	79
CZZ-811 (350)	80.0	10.0	10.0	–	Na_2CO_3	350	44

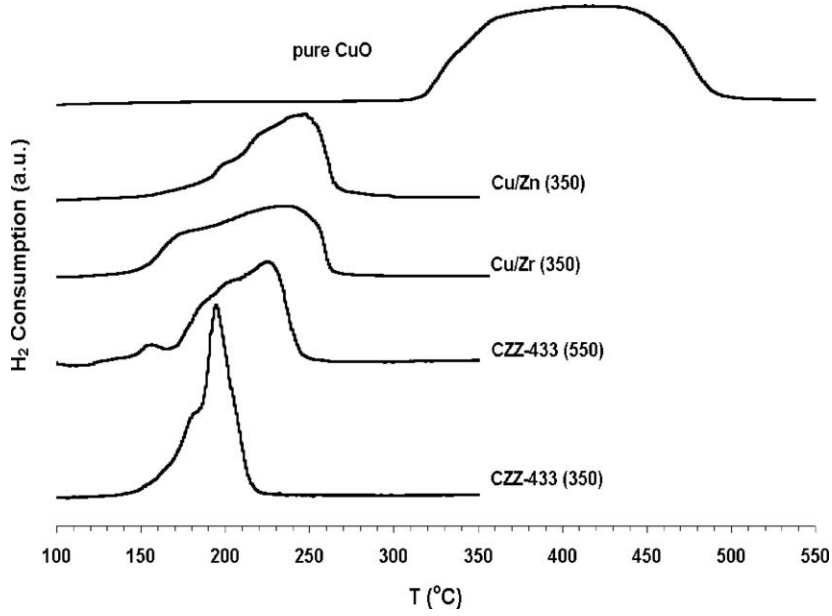

Fig. 1. Comparison of CuO reducibility in supported and unsupported samples as seen in TPR profiles.

area measurements are shown in Table 2. The amount of H_2 consumed during the initial reduction was used to determine the CuO weight percentage assuming that CuO was reduced to Cu^0. These values were found to be very close to "as-prepared" percentages. The measured Cu surface area was generally lower than expected based on the BET surface area and the Cu content of the catalysts. The values reported here are similar to other reports using the same technique [8,24]. Interestingly, the aluminum-containing catalyst had the highest Cu surface area. It is likely that sintering occurred during the initial reduction, thus decreasing the surface areas more for nonalumina catalysts. Sintering is known to be less drastic for samples containing alumina. Therefore, this method of measuring Cu surface area is biased toward

Table 2
Results from TPR and Cu surface area measurements

Catalyst	As prepared CuO (wt%)	CuO (wt%) from TPR	Cu SA (m^2/g)
Cu/Zn (350)	49	38	8.1
Cu/Zr (350)	39	44	0.4
Cu/Zr (550)	39	41	1.2
CZZ-244 (350)	16	18	5.6
CZZ-424 (350)	33	26	4.6
CZZ-433 (350)	34	34	10.6
CZZ-433 (550)	34	35	3.2
CZZA-433:0.5 (350)	33	27	16.9
CZZ-442 (350)	36	38	9.0
CZZ-811 (350)	76	69	0.1

samples that are more resistant to sintering during the reduction step, which reaches 350 °C. However, since sintering is a major cause of deactivation in Cu catalysts, this is still an effective method for identifying active catalysts that will be more stable. The next highest Cu surface area was for CZZ-433 (350). It should be noted that during N_2O passivation experiments some of the samples, especially those with extremely low measured Cu surface areas, decomposed N_2O to N_2 at a steady rate even after N_2O consumption decreased and leveled out. This slower N_2O decomposition could possibly be attributed to one of three causes: subsurface oxidation, full oxidation to CuO, or oxidation of mass-transfer-limited regions. Regardless of its source, this decomposition was not used in the calculation of Cu surface area since none of these three causes would correlate to active Cu sites.

3.3. XRD

In situ diffraction patterns were taken during calcination of CZZ-433 (350) and CZZ-244 (350), and reduction of CZZ-433 (350), CZZ-433 (550), CZZ-811 (350), and CZZA-433:0.5 (350). The calcination of CZZ-433 precursor is shown in Fig. 2. The corresponding *d* spacings and *hkl* values for the diffraction lines identified using EVA software and the ICDD PDF database are given in Table 3. The diffraction pattern of the initial light blue precipitate was observed to consist mostly of the aurichalcite $(Cu,Zn)_5(CO_3)_2(OH)_6$ phase, along with hydrozincite $Zn_5(CO_3)_2(OH)_6$ and malachite $Cu_2CO_3(OH)_2$ crystal structures (Fig. 2a). Since the most active catalyst was only calcined to 350 °C, it is interesting to note that the catalyst at this point was mostly amorphous with some crystallinity for the CuO and ZnO phases. This pattern matched the pattern of a sample subjected to a full 4 h of calcination. As the temperature increased (Fig. 2b), so did the crystallinity of CuO and ZnO, and at 500 °C crystalline ZrO_2 began to appear. Initially, ZrO_2 formed a possible rhombohedral phase at 500 °C, but eventually formed tetragonal

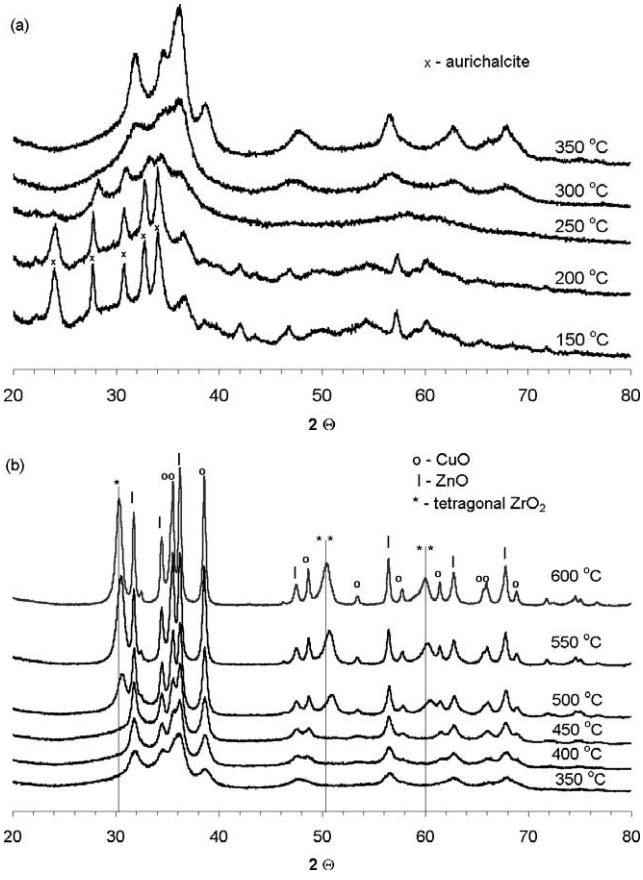

Fig. 2. In situ X-ray diffraction during calcination of CZZ-433 in air. (a) Precursor to catalyst transition (150–350 °C). (b) Catalyst crystallization (350–600 °C).

Table 3
Major peaks in the XRD patterns of identified phases during in situ calcination of CZZ-433 precursor

Phase	*d* (Å)	2Θ	*h*	*k*	*l*
Monoclinic	3.696	24.05	3	1	0
$Zn_3Cu_2(OH)_6(CO_3)_2$	3.262	27.32	−3	1	1
aurichalcite	3.262	27.32	2	1	1
	3.210	27.77	0	2	0
	3.126	28.53	−4	0	1
	3.126	28.53	3	0	1
	2.901	30.80	2	2	7
	2.811	31.81	−4	1	1
	2.811	31.81	3	1	1
	2.730	32.78	−1	2	1
	2.730	32.78	0	2	1
	2.645	33.86	−1	0	2
	2.626	34.12	−2	2	1
	2.626	34.12	1	2	1
	2.619	34.21	4	0	1
	2.619	34.21	4	0	3
Monoclinic	2.529	35.46	0	0	2
CuO copper	2.522	35.56	−1	1	1
oxide	2.321	38.77	1	1	1
	2.309	38.97	2	0	0
	1.867	48.74	−2	0	2
	1.710	53.53	0	2	0
	1.580	58.37	2	0	2
	1.505	61.56	−1	1	3
	1.417	65.87	0	2	2
	1.409	66.29	−3	1	1
	1.378	67.98	1	1	3
	1.374	68.17	2	2	0
Hexagonal	2.815	31.77	1	0	0
ZnO zinc	2.603	34.42	0	0	2
oxide	2.476	36.25	1	0	1
	1.911	47.54	1	0	2
	1.625	56.59	1	1	0
	1.477	62.87	1	0	3
	1.378	67.95	1	1	2
	1.359	69.08	2	0	1
Tetragonal	2.951	30.26	1	0	1
ZrO_2 zirconium	1.813	50.28	1	1	2
oxide	1.796	50.80	2	0	0
	1.556	59.35	1	0	3
	1.534	60.28	2	1	1

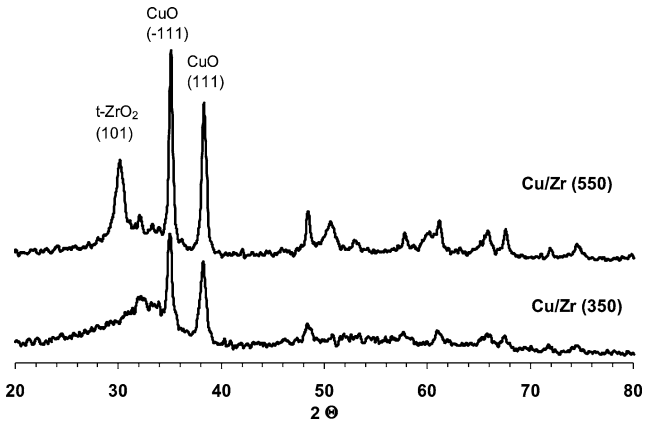

Fig. 3. Comparison of XRD patterns of Cu/Zr samples calcined at different temperatures in air.

ZrO_2 by 550 °C. The vertical lines in the figure help illustrate the shift occurring in the ZrO_2 pattern during the phase transition. The resulting postcalcined material was a dark brown color. As expected the only significant difference in the precursor to catalyst transition for CZZ-433 (350) and CZZ-244 (350) (not shown) was the intensity of the CuO peaks formed.

All of the postcalcined catalysts contained CuO and ZnO phases except the Cu/Zr samples, which do not contain ZnO. Samples calcined below 500 °C did not contain any detectable crystalline ZrO_2, while those calcined at 550 °C contained tetragonal ZrO_2. The clearest differences between calcination temperatures are seen for Cu/Zr (350) and Cu/Zr (550), as shown in Fig. 3. After calcining at 550 °C, Cu/Zr (550) contains tetragonal ZrO_2 and larger CuO crystals. Attempts were made to precipitate ZrO_2 by itself in order to better characterize the amorphous phase; however, a colloidal suspension formed which could not be washed by suction filtration, and upon drying at 100 °C a white amorphous gel formed. TPD and TGA/DSC studies summarized in the next sections offer more insight into the nature of the amorphous zirconia phase in the catalysts calcined at lower temperatures.

Diffraction patterns taken in situ during the reduction process show that reduction of the samples only changes the CuO phase to Cu, with no effect on ZnO or the respective zirconia phase. However, the degree of copper sintering that occurs during the reduction is dependent on the composition of the sample. Fig. 4 shows a comparison of the in situ X-ray diffraction patterns taken during reduction of CZZA-433:0.5 (350) and CZZ-811 (350), the samples with the highest and lowest measured Cu surface areas, respectively. It is likely that the sintering of CZZ-811 (350) during the reduction is the cause of its low measured Cu surface area. The alumina-containing material maintained its low crystallinity after the reduction; however, CZZ-811 (350) showed increased crystallinity with increasing temperatures. It is also interesting that for this sample adding a small amount of ZnO and ZrO_2 to CuO still improves reducibility as compared to pure CuO,

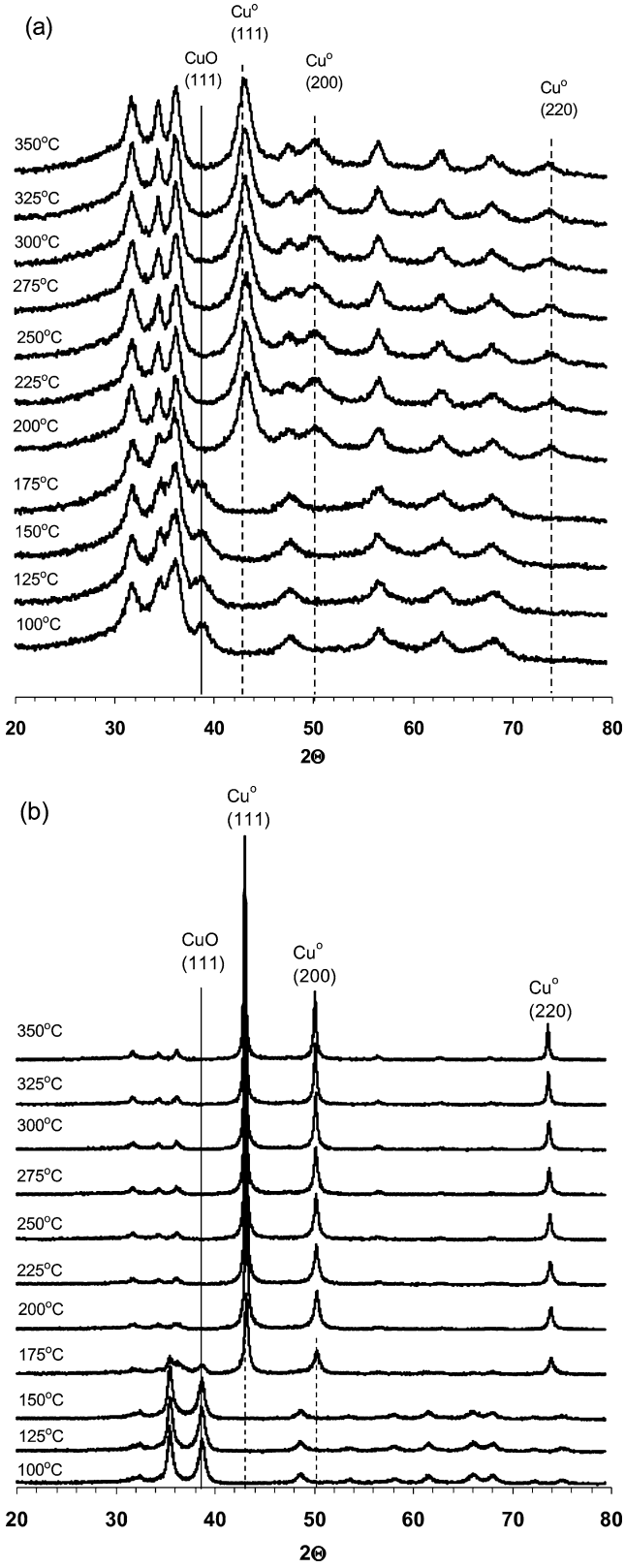

Fig. 4. In situ XRD patterns taken during reduction in 5% H_2 in N_2. (a) CZZA-433:0.5 (350). (b) CZZ-811 (350).

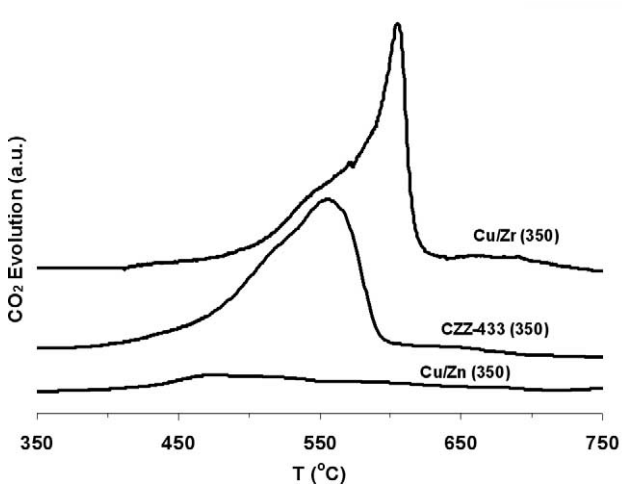

Fig. 5. Comparison of CO_2 evolution patterns during blank TPD.

but does not prevent sintering, showing the dual function of the supports in preventing sintering and improving reducibility of Cu. The reductions of CZZ-433 (350) and CZZ-433 (550) (not shown) were very similar to CZZA-433:0.5, except for the fact CZZ-433 (550) has a much sharper Cu^0 peak. This is because CuO is much more crystalline after calcining at the higher temperature, as was seen during in situ XRD calcination. Consequently, because of the higher degree of sintering, CZZ-433 (550) has a much lower Cu surface area than CZZ-433 (350) or CZZA-433:0.5 (350).

3.4. TPD

Blank temperature-programmed desorption experiments were carried out for calcined samples of Cu/Zn (350), Cu/Zr (350), and CZZ-433 (350). All of the samples containing the amorphous zirconia phase first released water over a broad range just above the calcination temperature of 350 °C, followed by CO_2 evolution beginning around 500 °C, which is approximately the same temperature crystalline ZrO_2 appears during in situ calcination. These features are likely the products of the decomposition of carbonates. Cu/Zn (350) released only a small amount of CO_2 in this temperature range, indicating that the CO_2 evolution is likely coming about from decomposition of the amorphous zirconia/zirconium carbonate in the zirconia-containing samples. A comparison of CO_2 evolution profiles for the samples is shown in Fig. 5. All of the samples released O_2 at high temperatures as Cu oxide begins to decompose. All samples were red/orange in color after the temperature treatment, indicative of metallic copper.

3.5. TGA/DSC

More insight on the precursor to catalyst transition and the nature of the amorphous zirconia phase can be obtained from TGA/DSC experiments. The products released during an in situ calcination (in He) of CZZ-433 precursor are

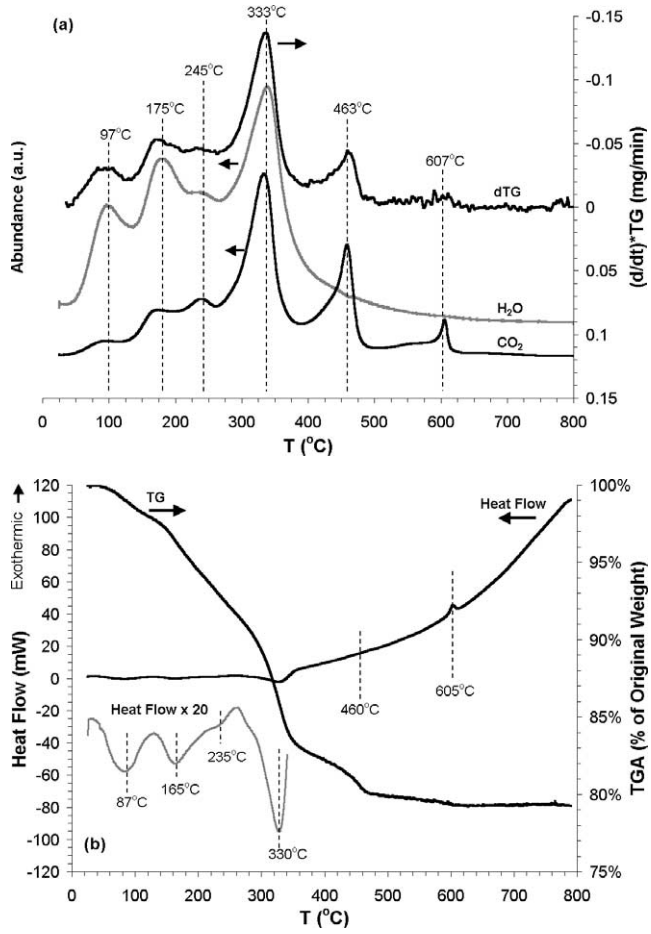

Fig. 6. TGA/DSC analysis of CZZ-433 precursor decomposition in helium. (a) The derivative of weight change with respect to time and the amount of CO_2 and H_2O released as a function of temperature. (b) Weight change and heat flow as a function of temperature.

graphed together with the derivative of the weight change with respect to temperature in Fig. 6a. Below 350 °C, the peak positions for weight change and CO_2 and H_2O released correlate nicely. The lower temperature peaks at 97 and 175 °C are most likely due to the loss of weakly adsorbed CO_2 and H_2O. Zirconia is known to release CO_2 and H_2O adsorbed from the atmosphere below 200 °C [33,34]. None of the Cu/Zn hydroxycarbonate species detected by XRD are known to decompose in this low temperature range; however, desorption of H_2O and CO_2 from these species is also possible in this temperature range. It should be noted that no changes in the XRD pattern were observed below 200 °C for a calcination in O_2. The peak at 245 °C (which has a higher CO_2 to H_2O ratio) likely originates from decomposition of hydrozincite to ZnO [35,36]. The large peaks at 333 °C can be attributed to the decomposition of aurichalcite, the main phase present in the precursor as detected by XRD [35,36]. DSC measurements presented in Fig. 6b confirm that these decompositions are endothermic, as reported by other researchers [35–37]. Malachite is known to decompose to CuO at 303 °C, so the shoulder preceding the

aurichalcite peaks may be attributed to a small amount of malachite [35,36].

Carbon dioxide is released endothermically at 463 °C without water. Only one CO_2 peak was observed during blank TPD experiments, so this CO_2 release may take place at lower temperatures in the presence of O_2. All of the possible Cu and/or Zn carbonate-containing phases are expected to decompose at lower temperatures [35–38], so this peak may be coming from a phase change in zirconia. The second smaller CO_2 peak begins just above 500 °C, and reaches a maximum at 607 °C. DSC shows a significant exothermic peak in the same region. This could be due to the release of heat from the exothermic crystallization of zirconia [34], but oxidation of carbonaceous species also is a possibility. At higher temperatures more heat is released presumably from sintering, showing how such sintering can be a self-perpetuating effect for these catalysts. Similar to blank TPD results, O_2 is released near 800 °C (not shown) from the reduction of CuO.

3.6. SRM reaction experiments

The results of reaction testing using equal weights of catalysts are shown in Fig. 7, where H_2 yield is defined as the percentage of the theoretical H_2 produced based on methanol fed assuming that 1 mol of methanol could react to form 3 mol of H_2. The SRM reactions were performed using an equal weight of catalyst in the reactor without a

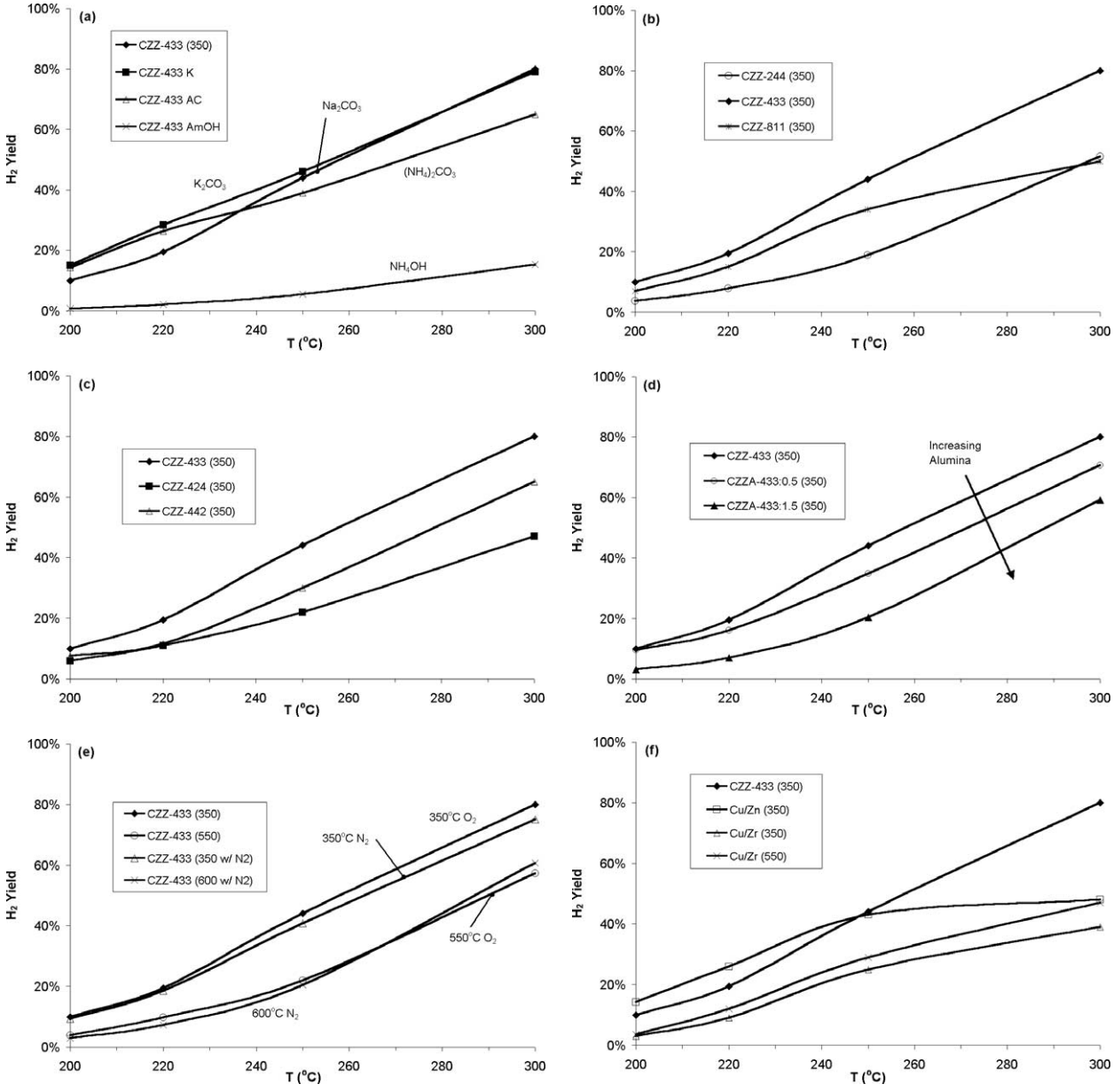

Fig. 7. Steam reforming of methanol reaction testing for unreduced catalysts (catalyst weight = 50 mg) showing effects of: (a) base used for precipitation, (b) Cu content, (c) Zn:Zr ratio, (d) addition of alumina, (e) calcination conditions, (f) composition.

prereduction step. The amount of CO by-product produced was always below the detectable limit for the TCD under these conditions, indicating that CO_2 selectivity was always greater than 99.8%. There was always CO detected by the FID using a methanizer; however, the concentrations were more of a function of methanol conversion rather than catalyst. Other researchers have reported trends in CO selectivity when methanol conversion was close to 100% for various catalyst compositions [28]. Methane product concentrations were always below 10 ppm and therefore undetectable. The FID with methanizer did detect small by-product concentrations of formaldehyde, formic acid, and methyl formate for all the samples; however, the concentration for any of these by-products was never more than 500 ppm.

The most active catalysts were prepared with 40 mol% of Cu precursors, and equal amounts of Zn and Zr precursors using a carbonate-containing base. This configuration also yielded the highest Cu surface area among non-alumina-containing samples. Using the alternative bases did not greatly affect the activity for steam reforming; however, when ammonium hydroxide was used, the resulting catalyst had slightly lower surface area and significantly lower activity (Fig. 7a). It is possible that some Cu was lost during filtration due to the formation of the soluble copper amine complex; however, the catalyst prepared with ammonium carbonate still performed quite well, suggesting that the low activity observed for the catalyst prepared with ammonium hydroxide was not simply due to the interaction of ammonia with copper. Although no Na or K was detected by XPS, it cannot be ruled out that these elements have a promoting effect considering their slightly higher activity. Ultimately, the formation of a hydroxycarbonate precursor seems to be the key to preparing an active catalyst. It is known for copper–zinc-based catalysts for the various reactions of interest that the decomposition of hydroxycarbonate precipitates leads to high surface area active catalysts in which Cu is well dispersed. Likewise, the formation of such precipitates was observed to be important in this series of catalysts as well.

Varying other pretreatment conditions had significant effects on activity. The effects of increasing copper content are observed when CZZ-244 (350), CZZ-433 (350), and CZZ-811 (350) are compared (Fig. 7b). Likewise, the effect of Zn:Zr ratio is observed when comparing CZZ-433 (350), CZZ-442 (350), and CZZ-424 (350) (Fig. 7c). The highest surface area and optimum activity by weight are obtained for CZZ-433 (350), which was also the sample with the highest measured Cu surface area of the group. The addition of aluminum decreased the activity of the sample. Even with its high BET and Cu surface areas, CZZA-433:0.5 (350) did not have better activity for the SRM reaction than CZZ-433 (350) (Fig. 7d). Others have reported that Al_2O_3 has an inhibiting effect for the SRM in prereduced Cu/ZnO-based catalysts [24,25]. Increasing the calcination temperature decreased activity (Fig. 7e) in addition to decreasing surface area and Cu surface area. Interestingly, samples calcined in the absence of oxygen still performed well, presumably because the hydroxycarbonate precursors decompose to form metal oxides even in an inert atmosphere.

The next most active catalyst on an equal weight basis, after CZZ-433 (350) and its derivatives, was Cu/Zn (350) (Fig. 7f), despite the fact that it had an extremely low surface area. Conversely, this catalyst had poor stability and lost activity when the reaction temperature was raised to 300 °C. This was most likely due to sintering of the copper. In commercial $Cu/ZnO/Al_2O_3$ low temperature shift catalysts, the addition of aluminum not only increases surface area but also decreases the rate of such sintering. Copper supported by zirconia maintained a high surface area when calcined at 350 °C and had good activity. Zirconia is known to be an effective support for copper for the methanol synthesis reaction, and steam reforming using prereduced catalysts, however, for steam reforming of methanol Cu/Zn (350) outperformed the Cu/Zr catalysts. Increasing the calcination temperature resulted in a decrease in surface area, but no loss in activity for Cu/Zr (550).

Overall it appears that CZZ-433 (350) is the best catalyst for several reasons. It was prepared with a carbonate base, making the formation of a hydroxycarbonate precursor possible, which is necessary for optimal activity since such a precipitate puts Cu and Zn in direct contact with one another. Additionally, this composition leads to the highest Cu surface area without the use of Al_2O_3, which would inhibit the reaction. Therefore, the high surface area with a large enough Cu content to yield a high Cu surface area, yet enough ZnO and ZrO_2 to prevent sintering, makes for a good SRM catalyst that apparently does not require prereduction to obtain good activity.

SRM reaction experiments were also performed by keeping the catalyst surface area in the reactor constant. By normalizing surface area in the reactor, a better idea can be obtained of how catalysts perform on a molecular level. From Fig. 8a it is apparent that CuO mixed with ZnO is the most active catalyst on an equal surface area basis. Unfortunately, this catalyst has a low surface area to begin with and suffers deactivation presumably due to sintering at increased temperatures, as was seen previously in equal weight measurements. Adding zirconia to Cu/ZnO, as in CZZ-433 (350), seems to provide better resistance to sintering. A comparison of catalysts with different compositions shows that CZZ-433 (350) is still the most active catalyst after Cu/Zn. It is interesting to note that on an equal surface area basis, the CZZ-433 catalysts calcined at different temperatures show the same activity (Fig. 8b). Another interesting point about the equal surface area comparisons is that Cu/Zr catalysts become more active when calcined at 550 °C. Methanol synthesis work has shown that copper supported by either a zirconia aerogel or a crystalline zirconia is active for the reverse of the reforming reaction. In fact, Jung and Bell even showed that the level of activity was dependent on which crystalline phase of zirconia was used [22]. Therefore, it is possible that tetragonal ZrO_2 present in Cu/Zr (550) is a more effective support for Cu than amorphous Zr. This would explain why

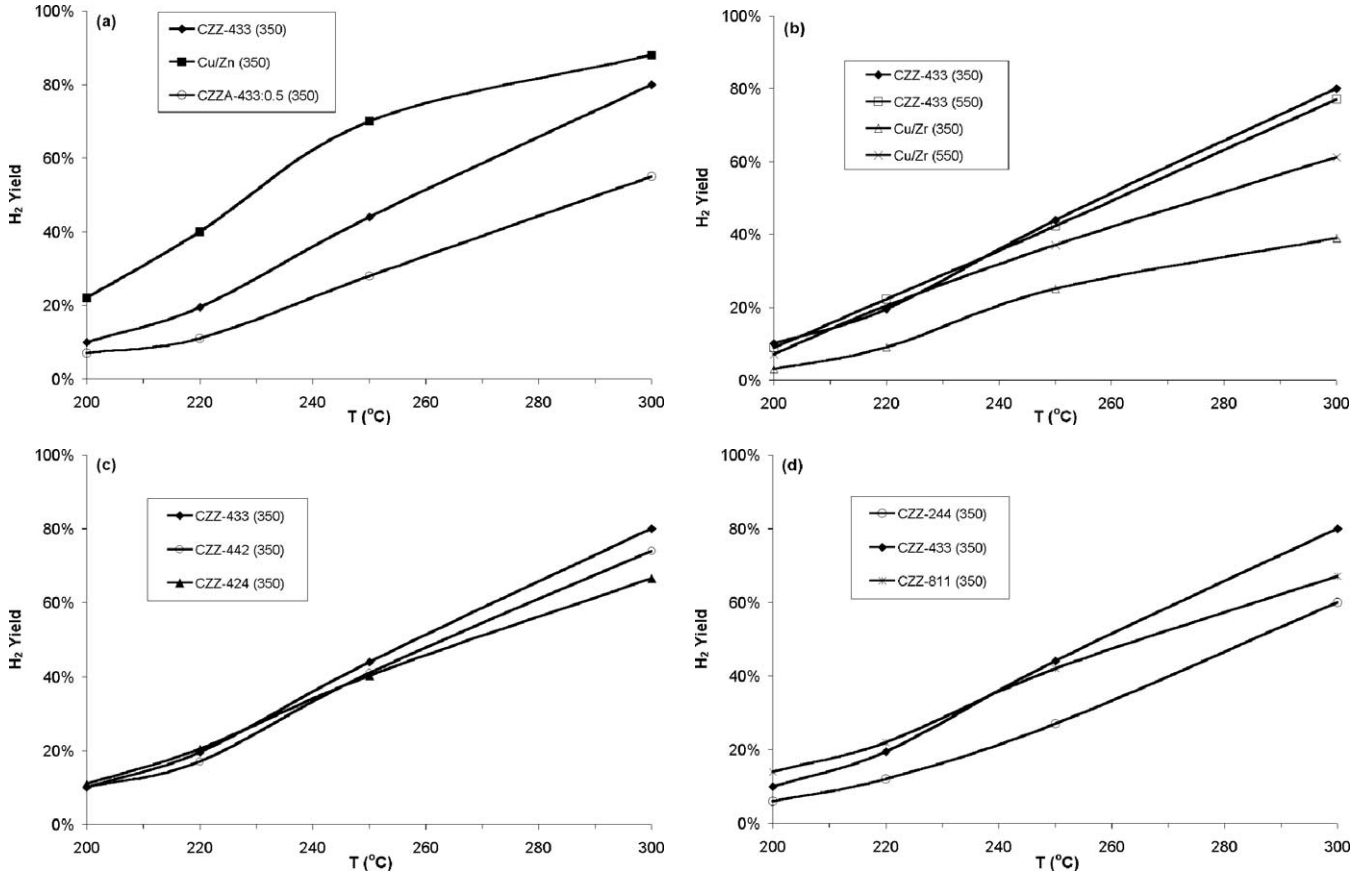

Fig. 8. Steam reforming of methanol reaction testing for unreduced catalysts (catalyst surface area = 4.4 m^2) showing effects of: (a) composition, (b) calcination temperature, (c) Zn:Zr ratio, (d) Cu content.

Cu/Zr (550) has the same activity as Cu/Zr (350) on an equal weight basis, despite having a lower surface area.

Figs. 8c and 8d confirm that CZZ-433 (350) is the optimal composition even on an equal surface area basis, as would be expected by Cu surface area measurements. Intuitively, one may think higher Cu content samples would perform better on an equal surface area basis if Cu is the source of activity; however, characterization showed that CZZ-811 is extremely prone to sintering and has a low Cu surface area. Samples prepared from carbonate bases have approximately the same BET surface area, and alumina-containing samples have a higher surface area than CZZ-433 (350); therefore, equal surface area testing was not performed on these samples.

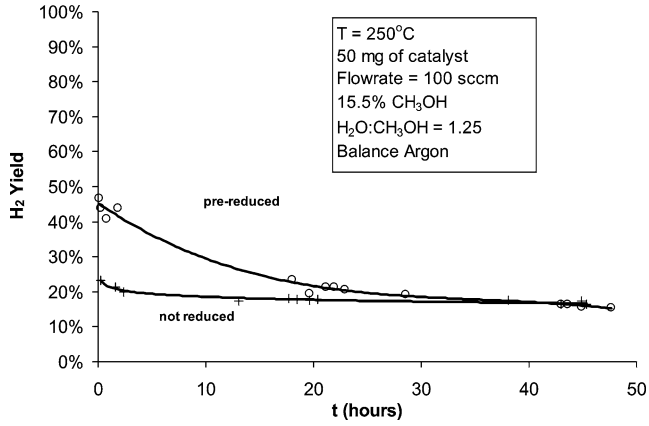

Fig. 9. Time-on-stream testing for CZZ-433 (550) comparing not reduced and prereduced samples.

3.7. Time-on-stream experiments

Activity testing as a function of time on stream showed that after an initial deactivation, the prereduced CZZ-433 (550) catalyst had the same activity as the nonreduced sample. Fig. 9 shows that the H_2 yield for the catalysts subjected to two different pretreatment conditions eventually converge. However, initially there is a large difference in activity for the two cases. Sintering effects and/or the slow oxidation of Cu may be playing a role in deactivation of the sample reduced with hydrogen [39]. For the purpose of this study, it is important to note that the effectiveness of a H_2 prereduction is dependent on the catalyst preparation parameters, and in the case of the best performing catalyst (CZZ-433 (350)), a H_2 prereduction seems unnecessary since the small difference in activity of prereduced and nonreduced samples vanishes quickly as the activities converge in under 4 h. The activities for samples containing alumina did

not converge, and the prereduced samples maintained higher activity even after 48 h of testing. Reasons for these observations will be discussed in more detail in the authors' next paper.

3.8. XPS

X-ray photoelectron spectra were obtained for samples with different compositions and/or different calcination temperatures. In addition to prereaction spectra, postreaction spectra were also obtained for the CZZ-433 (550) samples subjected to time-on-stream tests. Table 4 shows the binding energies and peak assignments of the identified peaks for calcined samples. After calcination, the phases present were consistently CuO along with ZnO and/or ZrO_2. Using a higher calcination temperature increased the BE for both ZnO and ZrO_2 peaks, while adding ZnO to ZrO_2 decreased the BE of ZrO_2 by approximately 0.5 eV.

Table 4
XPS results for untreated samples

Sample	Peak	BE (eV)
Cu/Zr (350)	Cu $2p_{3/2}$	933.6
	Zr $3d_{5/2}$	182.1
Cu/Zr (550)	Cu $2p_{3/2}$	933.6
	Zr $3d_{5/2}$	182.3
Cu/Zn (350)	Cu $2p_{3/2}$	933.7
	Zn $2p_{3/2}$	1021.9
	Cu $2p_{3/2}$	933.7
CZZ-433 (350)	Zn $2p_{3/2}$	1022.1
	Zr $3d_{5/2}$	181.7
	Cu $2p_{3/2}$	933.6
CZZ-433 (550)	Zn $2p_{3/2}$	1022.2
	Zr $3d_{5/2}$	181.9

As Fig. 10 shows, CuO is reduced by the reactants at the point in time when steady state has been reached. It is interesting to note that the X-ray photoelectron spectra of the postreaction samples are very similar for both prereduced and unreduced samples. This result is quite consistent with the observations made in the time-on-stream experiments which showed that the performance of the prereduced catalyst became identical to that of an unreduced sample after being on stream for about 30 h. The oxidation state of Cu in the postreaction samples cannot be determined definitely by XPS since the BE ranges of possible reduced states overlap. However, the binding energy of the postreaction sample was not as low as that of a fully reduced sample. Therefore, it is conceivable that the postreaction samples (regardless of their reduction history) contain reduced Cu once steady state is reached, but show signs of partial oxidation, subsurface oxidation, or even a higher oxidation state compared to fully reduced Cu^0. The other components remain unaffected, as seen by their binding energies shown in Table 5.

4. Conclusions

Characterization of the zirconia-containing Cu/ZnO-based catalysts showed that the catalysts calcined at 350 °C consisted of CuO, ZnO, and a high surface area amorphous zirconia phase. This amorphous phase releases CO_2 upon its

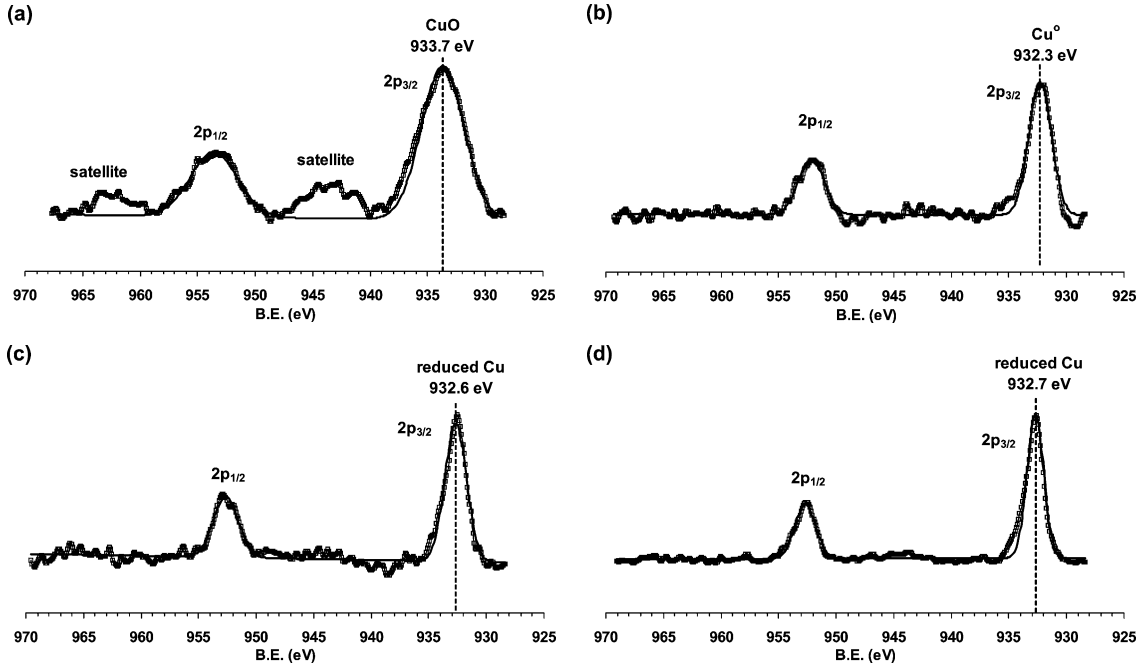

Fig. 10. XPS spectra of Cu 2p region for CZZ-433 (550) samples: (a) calcined (prereaction), (b) prereduced (prereaction), (c) calcined (postreaction), (d) prereduced (postreaction).

Table 5
XPS results for CZZ-433 (550) after being subjected to various conditions

Treatment history	Peak	BE (eV)
Reduced	Cu $2p_{3/2}$	932.3
	Zn $2p_{3/2}$	1022.2
	Zr $3d_{5/2}$	182.5
Postreaction	Cu $2p_{3/2}$	932.6
	Zn $2p_{3/2}$	1022.4
	Zr $3d_{5/2}$	182.2
Reduced postreaction	Cu $2p_{3/2}$	932.7
	Zn $2p_{3/2}$	1022.4
	Zr $3d_{5/2}$	182.5

crystallization to a lower surface area tetragonal ZrO_2 phase at temperatures near 500 °C.

Reaction testing showed that prereduction is not necessary to activate these catalysts and only provides temporary improved activity in the case of nonalumina samples. In accord with previous studies on prereduced zirconia-containing Cu/ZnO SRM catalysts, the most active nonreduced catalysts contained the high surface area amorphous zirconium phase and an optimal amount of CuO and ZnO to allow for high Cu surface area. From Cu surface area results it can be rationalized that this catalyst has good resistance to sintering compared to the poor performing samples. Although alumina increased Cu surface area, it had an apparently negative effect on SRM activity for nonreduced samples.

Postreaction XPS experiments indicated that CuO in an oxidized catalyst can be at least partially reduced by the reaction mixture, and a prereduced catalyst becomes partially oxidized. The results of in situ characterization of these non-reduced catalysts in SRM reaction conditions will be presented in the next paper in this series.

References

[1] S. Ahmed, M. Krumpelt, Int. J. Hydrogen Energy 26 (2001) 291.
[2] H.H. Kung, Catal. Rev.-Sci. Eng. 22 (1980) 235.
[3] M.S. Wainwright, D.L. Trimm, Catal. Today 23 (1995) 29.
[4] T. Fujitani, J. Nakamurs, Catal. Lett. 56 (1998) 119.
[5] M. Bowker, R.A. Hadden, H. Houghton, J.N.K. Hyland, K.C. Waugh, J. Catal. 109 (1988) 263.
[6] C. Rhodes, G.J. Hutchings, A.M. Ward, Catal. Today 23 (1995) 43.
[7] K.M. Vanden Bussche, G.F. Froment, J. Catal. 161 (1996) 1.
[8] L. Alejo, R. Lago, M.A. Pena, J.L.G. Fierro, Appl. Catal. A 162 (1997) 281.
[9] B.A. Peppley, J.C. Amphlett, L.M. Kearns, R.F. Mann, Appl. Catal. A 179 (1999) 31.
[10] T.-J. Huang, S.-W. Wang, Appl. Catal. 24 (1986) 287.
[11] T.L. Reitz, S. Ahmed, M. Krumpelt, R. Kumar, H.H. Kung, J. Mol. Catal. A 162 (2000) 275.
[12] C. Jiang, D.L. Trimm, M.S. Wainwright, Appl. Catal. A 93 (1993) 245.
[13] T.L. Reitz, P.L. Lee, K.F. Czaplewski, J.C. Lang, K.E. Popp, H.H. Kung, J. Catal. 199 (2001) 193.
[14] S. Velu, K. Suzuki, T. Osaki, Chem. Commun. (1999) 2341.
[15] S. Velu, K. Suzuki, T. Osaki, Catal. Lett. 62 (1999) 159.
[16] B.A. Peppley, J.C. Amphlett, L.M. Kearns, R.F. Mann, Appl. Catal. A 179 (1999) 21.
[17] C.P. Thurgood, J.C. Amphlett, R.F. Mann, B.A. Peppley, Top. Catal. 22 (2003) 253.
[18] G. Fierro, M. Lo Jacono, M. Inversi, P. Porta, F. Cioci, R. Lavecchia, Appl. Catal. A 137 (1996) 327.
[19] D. Duprez, J. Barbier, Z. Ferhat-Hamida, M. Bettahar, Appl. Catal. 12 (1984) 219.
[20] D. Duprez, Z. Ferhat-Hamida, M.M. Bettahar, J. Catal. 124 (1990) 1.
[21] Y. Nitta, O. Suwata, Y. Ikeda, Y. Okamoto, T. Imanaka, Catal. Lett. (1994) 345.
[22] K.T. Jung, A.T. Bell, Catal. Lett. 80 (2002) 63.
[23] D. Bianchi, T. Chafik, M. Khalfallah, S.J. Teichner, Appl. Catal. A 105 (1993) 223.
[24] J.P. Breen, J.R.H. Ross, Catal. Today 51 (1999) 521.
[25] S. Velu, K. Suzuki, M. Okazaki, M.P. Kapoor, T. Osaki, F. Ohashi, J. Catal. 194 (2000) 273.
[26] B. Lindstrom, L.J. Pettersson, Int. J. Hydrogen Energy 26 (2001) 923.
[27] X.R. Zhang, P. Shi, J. Zhao, M. Zhao, C. Liu, Fuel Process. Technol. 83 (2003) 183.
[28] J. Agrell, H. Birgersson, M. Boutonnet, I. Melian-Cabrera, R.M. Navarro, J.L.G. Fierro, J. Catal. 219 (2003) 389.
[29] U.S. Ozkan, Y. Cai, M. Kumthekar, L. Zhang, J. Catal. 142 (1993) 182.
[30] M.J. Luys, P.H. Van Oeffelt, W.G.J. Brouwer, A.P. Pijpers, J.J.F. Scholten, Appl. Catal. 46 (1989) 161.
[31] G.C. Bond, S.N. Namijo, J. Catal. 118 (1989) 507.
[32] J.W. Evans, M.S. Wainwright, A.J. Bridgewater, D.J. Young, Appl. Catal. 7 (1983) 75.
[33] J. Nawrocki, P.W. Carr, M.J. Annen, S. Froelicher, Anal. Chim. Acta 327 (1996) 261.
[34] G. Stefanic, S. Popovic, S. Music, Thermochim. Acta 259 (1995) 225.
[35] G.-C. Shen, S. Fujita, S. Matsumoto, N. Takezawa, J. Mol. Catal. A: Chem. 124 (1997) 123.
[36] P. Porta, S. De Rossi, G. Ferraris, M. Lo Jacono, G. Minelli, G. Moretti, J. Catal. 109 (1988) 367.
[37] N. Kanari, D. Mishra, I. Gaballah, B. Dupre, Thermochim. Acta 410 (2004) 93.
[38] Z. Ding, R. Frost, J.T. Kloprogge, J. Mater. Sci. Lett. 21 (2002) 981.
[39] M.V. Twigg, M.S. Spencer, Top. Catal. 22 (2003) 191.